Title
WAT-on-a-chip: a physiologically relevant microfluidic system incorporating white adipose tissue.

Journal
Lab on a chip, 17(9)

ISSN
1473-0197

Authors
Loskill, Peter
Sezhian, Thiagarajan
Tharp, Kevin M
et al.

Publication Date
2017-05-01

DOI
10.1039/c6lc01590e

Peer reviewed

HHS Public Access

Author manuscript

Lab Chip. Author manuscript; available in PMC 2018 May 02.

Published in final edited form as:

Lab Chip. 2017 May 02; 17(9): 1645–1654. doi:10.1039/c6lc01590e.

WAT-on-a-chip: A physiologically relevant microfluidic system incorporating white adipose tissue

Peter Loskill[a,b,#], **Thiagarajan Sezhian**[b], **Kevin Tharp**[c], **Felipe T. Lee-Montiel**[a,b], **Shaheen Jeeawoody**[a], **Willie Mae Reese**[b], **Pete-James H. Zushin**[c], **Andreas Stahl**[c,*], and **Kevin E. Healy**[a,b,*]

[a]Department of Bioengineering and California Institute for Quantitative Biosciences (QB3), University of California at Berkeley, Berkeley, California 94720, USA

[b]Department of Materials Science and Engineering, University of California at Berkeley, Berkeley, California 94720, USA

[c]Department of Nutritional Sciences & Toxicology, University of California at Berkeley, Berkeley, California 94720, USA

Abstract

Organ-on-a-chip systems possess a promising future as drug screening assays and as testbeds for disease modeling in the context of both single-organ systems and multi-organ-chips. Although it comprises approximately one fourth of the body weight of a healthy human, an organ frequently overlooked in this context is white adipose tissue (WAT). WAT-on-a-chip systems are required to create safety profiles of a large number of drugs due to their interactions with adipose tissue and other organs via paracrine signals, fatty acid release, and drug levels through sequestration. We report a WAT-on-a-chip system with a footprint of less than 1 mm^2 consisting of a separate media channel and WAT chamber connected via small micropores. Analogous to the in vivo blood circulation, convective transport is thereby confined to the vasculature-like structures and the tissues protected from shear stresses. Numerical and analytical modeling revealed that the flow rates in the WAT chambers are less than 1/100 of the input flow rate. Using optimized injection parameters, we were able to inject pre-adipocytes, which subsequently formed adipose tissue featuring fully functional lipid metabolism. The physiologically relevant microfluidic environment of the WAT-chip supported long term culture of the functional adipose tissue for more than two weeks. Due to its physiological, highly controlled, and computationally predictable character, the system has the potential to be a powerful tool for the study of adipose tissue associated diseases such as obesity and type 2 diabetes.

Correspondence Address: Kevin E. Healy, 370 Hearst Memorial Mining Bldg., #1760, University of Berkeley, Berkeley, CA 94720-1760, kehealy@berkeley.edu. Andreas Stahl, 119 Morgan Hall, #3104, University of California Berkeley, Berkeley, CA 94720-3104, astahl@berkeley.edu.

[#]Present address: Department of Cell and Tissue Engineering, Fraunhofer Institute for Interfacial Engineering and Biotechnology (IGB), 70569 Stuttgart, Germany.

Disclosure Statement

KEH is has a financial relationship with Organos Inc. and both he and the company may benefit from commercialization of the results of this research.

Introduction

Engineered tissues have emerged as a powerful tool for translational biomedical applications as well as to understand and study disease mechanisms. Although various tissue engineering approaches for regenerative medicine have been introduced,[1,2] they typically have restricted usefulness for other applications such as drug screening due to three major limitations. First, currently they cannot recapitulate the complex circulation of humans which continuously transports nutrients, drugs, and other soluble compounds toward the tissue, and clears metabolic waste away from the tissue. Second, their macroscale requires a large number of cells preventing the parallelization and scale up for commercial applications. Third, they typically have tissue to fluid volume ratios that are not physiologic thereby altering the delicate balance of autocrine and paracrine factors on tissue function. These limitations can be overcome by integrating engineered tissue with physiologically relevant microfluidic systems to create organ-on-a-chip systems, which have evolved from a conceptual idea to a feasible new paradigm for drug screening.[3–8] These microfluidic approaches offer significant advances including: unprecedented control of fluid flows; compatibility with high content drug screening; miniaturization of large systems for convenient operation; significant reduction of very expensive cell reagents used; physiological relevant tissue to media volumes, and potential for connection with other organ systems. Recently, a variety of promising organ-on-a-chip systems have been developed, also referred to as microphysiological systems (MPS), such as models of cardiac,[9] pulmonary,[10] hepatic,[11] renal,[12] and vascular tissues.[13]

In spite of it comprising approximately 20% body weight of healthy men and up to 25% women, and can reach more than 50% body weight in obese adults,[14,15] adipose tissue has been frequently overlooked for MPS. Like the liver and skeletal muscle, white adipose tissue (WAT) is an insulin sensitive organ as well as a critical storage site for excess dietary energy. WAT exists in different anatomical locations and is comprised of a heterogeneous collection of cell types that are dominated by unilocular adipocytes. WAT depots not only serve as storage sites for triacylglycerol, but also have been established as a major endocrine organ secreting a variety of cytokines, termed adipokines.[16–18] Adipokines, such as leptin and adiponectin, are known to play significant roles in a variety of human diseases and loss of all WAT, as is observed in patients with lipodystrophy, leads to severe metabolic and endocrine abnormalities. [19–22] Adiponectin concentrations have, for instance, been shown to affect organs such as liver,[23] heart,[24] and kidney.[25] Furthermore, the potential of adipose tissue as a direct target for pharmacotherapies is becoming recognized,[26] especially in the context of rapidly increasing prevalence of adipose-related diseases such as obesity and type 2 diabetes. The Centers for Disease Control and Prevention, for instance, reported in 2012 that more than 35% of U.S. adults suffered from obesity.[27] Besides the direct involvement in diseases or as a drug target, the storage character of WAT provides a further key aspect. Plasma concentrations of drug compounds and drug exposure kinetics *in vivo* are strongly affected by the “ADME” processes – absorption, distribution, metabolism, and excretion. As WAT is known to sequester hydrophobic drug compounds,[28,29] a WAT-on-a-chip is of utmost importance in the endeavor to mimic *in vivo* ADME properties in integrated multi-organ MPS.

In recent years, a variety of engineered adipose tissue constructs have been introduced.[14] The majority incorporated adipocytes into three dimensional scaffolds consisting of various biomaterials,[30] using for instance collagen/alginate,[31] silk fibroin,[32] porous polymers,[33], decellularized extracellular matrices,[34] or bioinspired matrices.[35] While these systems have a potential as implants for regenerative medicine, their use as *in vitro* models is restricted by the limitations mentioned above. One of the limitations, the lack of circulation, was successfully addressed by incorporating the tissue constructs into macroscopic bioreactors,[36,37] which were successfully downscaled to cm size reactors connected to microfluidic channels.[38] Initial attempts to create microscale, microfluidic systems for the culture of white adipose tissue have also been reported.[39–41] These attempts used initially open systems, which were closed subsequent to seeding cells or inserting entire cover slides into them. While this approach elegantly circumvents the challenge of inserting fragile and buoyant adipocytes into microscale chambers, it limits the potential for further downscaling, parallelization for high content screening and integration with other systems. Additionally, although these systems succeeded in establishing a continuous flow environment, the degree of structural mimicry of the *in vivo* physiology is limited and they specifically fail in protecting the tissue from shear stresses, thereby missing a key element of the *in vivo* vasculature.

Here we present a WAT-on-a-chip system that creates a physiologically relevant microfluidic environment enabling the control of nanoliter fluid volumes and flows that are unavailable with other methods. The system consists of separate media channel and WAT chambers, which are connected via small micropores. Analogous to the in vivo blood circulation, convective transport is thereby confined to the vasculature-like channel. The WAT chamber hence provides a recapitulated native physiological niche protected from shear forces by an endothelial-like barrier in which adipocytes can be injected and supported for long term culture to produce functional adipose tissue.

Materials and Methods

Fabrication and characterization of WAT-chip

The multilayer WAT-chip consists of two patterned polydimethylsiloxane (PDMS, Sylgard 184) slabs sandwiching a polyethylene terephthalate (PET) membrane (r_P = 3 μm; ρ_P = 8 10^5 pores/cm^2; AR Brown-US, Pittsburgh, PA. To generate the PDMS slabs, patterned master-wafers were fabricated via a photolithography process. Thereto, a 50 μm thick layer of SU-8 3050 photoresist (MichroChem Corp, Newton, MA) was spin coated onto silicon wafers (University Wafer, Boston, MA) and exposed to UV light through patterned transparency masks according to the manufacturer's data sheet. Wafers were developed in SU-8 developer (MichroChem Corp, Newton, MA), rinsed in isopropanol, and blow dried with N2. The patterned wafers were baked, and coated with trichloro-1H, 1H, 2H, 2H-perfluorooctylsilane (FOTS, Gelest, PA, USA). The masks for both wafers were designed in AutoCAD LT (Autodesk Inc., San Rafael, CA). PDMS slabs were then replica molded using uncured PDMS in a 10:1 w/w ratio of prepolymer to curing agent. To mold the slab featuring the media channel a total of 11 g of PDMS was poured onto the wafer and cured overnight at 60°C. Similarly, the slab featuring the cell chamber was molded using 30 g of

PDMS. After peeling the molds from the wafers, inlet/outlet holes were punched in the cell chamber PDMS slab using a 0.75 mm biopsy punch (Ted Pella).

To prepare the isoporous PET membranes, they were cut to appropriate dimensions and cleaned through sonication in isopropyl alcohol for 10 minutes. The membranes were then exposed to oxygen plasma (Plasma Equipment Technical Services, Livermore, CA) at 60 W for 60 s. The activated membranes were incubated in a solution of 97% isopropyl alcohol, 2% bis(3-(trimethoxysilil)propyl)amine and 1% Milli-Q Water at 80°C for 20 minutes and subsequently rinsed with isopropyl alcohol. After drying at 80°C for 30 minutes, the membranes were placed in 2 mL of 70% ethanol in Milli-Q water.

To assemble the multi-layer PET/PDMS hybrid device, the unpatterned backside of the PDMS slab featuring media channels was bonded to a microscope glass slide after exposure to oxygen plasma at 60 W for 20 s. The patterned faces of both PDMS slabs were then once more exposed to oxygen plasma at 60 W for 20 s and sandwiched around the previously functionalized PET membrane, which was carefully blow dried with N_2. To ensure a proper alignment of media channel with cell chambers, the assembly was performed under a stereomicroscope. To stabilize bonding, the devices were subsequently baked overnight at 80°C.

For the assessment of sealing and fluidic connection, both media channel and cell chambers were first prefilled with red food dye (DecACake) coloured Milli-Q water followed by pumping blue coloured Milli-Q water through the media channels. Color movies were taken using a Leica M80 stereomicroscope (Leica, Wetzlar, Germany) system equipped with a Leica MC170 camera.

Numerical modeling

COMSOL Multiphysics (COMSOL, Stockholm, Sweden) was used to model fluid flow and transport of a diluted species. Treating the membrane as an array of cylindrical pores could not be achieved due to computational memory limitations. To overcome this barrier, we employed a finite element model treating the membrane as a porous media as described previously.[42] Briefly, the flow through the membrane was solved using the time-dependent solver with a *finer* physics controlled mesh. The iterative solver was employed using multigrid methods to further overcome computational limitations. The “Free and Porous Flow” module engaged the Navier-Stoke equation to solve for the free flow of the media through the cell and media channels and Darcy’s Law to solve for the flow of media through the membrane, modeled as a porous medium. The membranes used have a porosity of ~5.6%, pore radius of 1.5 μm, and a thickness or pore length of 20 μm. The fluidic resistance of the pores was calculated to $R_P = 1.097 \times 10^{16}$ Ns/m^6 by employing Dagan’s equation,[43] which solves for the entrance and exit effects through a short pore via

$$R_P = \frac{\mu}{r_P^3}\left(3 + \frac{8}{\pi}\frac{L}{r_P}\right)$$

with fluid viscosity μ, pore radius r_P, and pore length L. The hydraulic permeability K was calculated to K = 1.45 × 10^{-14} m^2 using

$$K=\frac{\mu L \rho}{\pi r_P^2 R_p}$$

whereby ρ is the porosity of the membrane. Simulations are conducted with a media flow rate of 5.56 × 10^{-12} m^3/s (20 μL/h).

Additionally, the “Transport of Dilute Species” module was used to assess the ability of the membrane to allow for the diffusion of small molecules solved in the media. Therefore, the media channel is pre-filled at time point zero with “media” containing a species c in a concentration of 1 μM and constantly perfused with the same media at 20 μL/h. When assuming a typical diffusion coefficient of 1 × 10^{-9} m^2/s for a biological molecule in water,[44] the concentration of the species in most of the cell chamber reaches the initial concentration of 1 μM within 30 seconds.

Analytical model

The analytical model approximates the membrane as an idealized system with pores in a hexagonally close packed arrangement with rows of pores aligned with the direction of media flow and a pore-to-pore distance of

$$L_P=\sqrt{\frac{\pi * r_p^2}{\sin 60\, p_M}}$$

with the membrane porosity p_M and the pore radius r_P. In this system, the flow in the channels can be solved using an electrical circuit analogy involving the resistance of the pores R_P, the resistances of the media and cell channel R_m and R_c respectively, and the input flow rate Q (Fig. 3E).[42] Applying this analogy to unit segments of length L_P, a generalized recurrence relation can be obtained whereby the flow rate in the n^{th} segment of the tissue chamber (with a total of N segments) is

$$q_c(n)=Q\frac{R'_m}{R'_m+R'_c}(1-\omega(n))$$

with

$$\omega(n)=\frac{e^{\beta n}}{e^{\beta}+e^{\beta N}}+\frac{e^{-\beta n}}{e^{-\beta}+e^{-\beta N}}$$

and

$$\beta=\cosh^{-1}\left(\frac{2R'_P+R'_m+R'_c}{2R'_P}\right).$$

The derivation of these formulas is similar to the one reported by Chung *et al.* with the difference that due to the circular structure of media and cell chamber, the width of the channel is different for each segment. Hence, all resistances R_P, R_M and R_C in principle depend on the chamber width *w* and the segment index *n* respectively. However, as elucidated in the following these formulas can nevertheless be applied to the system by using a slight modification.

The total pore resistance of a membrane cross-section perpendicular to the media flow consisting of multiple identical pores is

$$R_P(w)=\frac{R_{SP}}{N_{PW}(w)}$$

with the resistance of a single pore R_{SP} and the number of pores per cross-section $N_{PW}(w)=\frac{w}{L_P\sin 60}$. R_{SP} can thereby be calculated using Dagan's equation, which accounts for edge effects for flow through a short through pore,

$$R_{SP}=\frac{\mu}{r_P^3}\left[3+\frac{8}{\pi}\frac{h_M}{r_P}\right]$$

with the fluid viscosity μ and the membrane thickness (pore length) h_M. By defining projected resistances R′ with $R_P(w)=\frac{R'_P}{w}$ as well as $R_c(w)=\frac{12\mu L_P}{h_c^3 w}=\frac{R'_C}{w}$ and $R_m(w)=\frac{12\mu L_P}{h_m^3 w}=\frac{R'_m}{w}$ respectively (Hagen–Poiseuille equation of flow in rectangular channels) and considering the fact that solely ratios of resistances occur in the formulas, we can cancel out the width dependence and replace resistances R in the equations from Chung *et al.* with projected resistances R′. By looking at the derivative $\frac{dq_C}{dn}$ it becomes obvious that the maximum flow in the cell chamber occurs at n = 0.5*N.

Cell culture and differentiation

3T3-L1 fibroblasts (ATCC) were differentiated as described previously.[45] Briefly, fibroblasts were cultured in DMEM medium containing 10% fetal bovine serum with 2 mM l-glutamine and 1% penicillin/streptomycin (DMEM/FBS). To induce adipogenesis, the cells were cultured in DMEM/FBS for 2 days after reaching confluence and then for 2 days in DMEM/FBS supplemented with 5 μg/mL (0.86 μM) insulin, 0.25 μM dexamethasone, and 0.25 mM isobutylmethylxanthine. Subsequently, the medium was changed to DMEM/FBS supplemented solely with 5 μg/mL insulin and the cell cultured for an additional 2 days. Finally, the cells were maintained in DMEM/FBS alone. Differentiated cells (at least 95% of

which showed an adipocyte phenotype by accumulation of lipid droplets) were injected into the MPSs on days 6–10 after initiation of differentiation.

Cell Loading

To ensure a successful loading of the MPSs, differentiated adipocytes were singularized and maintained in suspension by treatment with 0.5% trypsin w/ EDTA for 2 min, detached from the surface, and then suspended in DMEM/FBS media. The suspension was subsequently centrifuged for 5 min at 400 g and the diluted trypsin aspirated off. After that, the cells were resuspended in fresh media such that a solution of 3–5 million cells/mL was obtained and the loading process started immediately.

To prepare the loading process, fully assembled MPSs were exposed to O_2 plasma at 180 W for 1 minute thereby sterilizing and creating more hydrophilic channel surfaces. Immediately thereafter, 100–200 mL of cell solution was applied to the cell inlet ports of the MPSs, which were then stored for 15 min in the incubator to allow for sedimentation of cells resulting in a high cell density inside the inlet ports. By applying a negative pressure to the cell media inlet and outlet port using a PhD Ultra syringe pump (Harvard Apparatus) cells were loaded into the cell chamber until a densely packed cell pellet was obtained. Subsequent to the actual loading step, the MPSs were stored for 30 min in the incubator to allow cell attachment before starting the flow of media through the media channels. The media flow was achieved using a PhD Ultra syringe pump at a flow rate of 20 μL/h.

On-chip culture and characterization

To asses viability of the WAT on chip, Live/Dead cytotoxicity assays were performed using a LIVE/DEAD cell imaging kit (Molecular Probes R37601) to stain viable cells with green-fluorescent calcein AM (488nm) and dead cells with red ethidium homodimer-1 (570nm). The live/dead imaging kit was used following the manufacturer protocol: 3T3-L1 cells in WAT chips were rinsed with PBS 1X and 60 μL of dye was added to the devices and then incubated for 20 min. After this incubation time, images were collected using an inverted microscope Nikon TE300 with a Lumencore Spectra X light engine. Images were then processed in FIJI ImageJ. Utilizing segmentation analyses and a constant area exclusion filter counts of live or dead cells were obtained. An index of cell death was constructed from the ratio of the number of dead cell events divided by total number of cells.

For long-term culture, loaded MPSs were stored in the incubator and fed by a PhD Ultra syringe pump with continuous media flow. For visual characterization, cells were imaged daily without detachment from the syringe pump using a Nikon Eclipse TE300 microscope. To better visualize the lipid droplets, cells were stained using a nonpolar fluorophore specific for neutral lipids. Thereto, MPSs were incubated overnight at 4°C in a 4% solution of paraformaldehyde (Santa Cruz Biotechnology). Subsequently, a solution of PBS with 0.1% Tween (PBST) was flushed through the MPSs for 3 h followed by a 2h flush with PBST containing 1 μg/mL 4,4-difluoro-1,3,5,7,8-pentamethyl-4-bora-3a,4a-diaza-s-indacene (BODIPY D-3922, Molecular Probes, Eugene, OR) and 300 nM 4′,6-diamidino-2-phenylindole (DAPI, Molecular Probes). After a final washing step with PBS, the MPSs were imaged with a Zeiss LSM710 laser-scanning microscope (Carl Zeiss, Jena, Germany).

To characterize the uptake functionality of the adipocytes in the MPS after two weeks in-chip culture, the cells were fed with a fluorescently-labeled fatty acid analog. DMEM/FBS media was supplemented with 4μM 4,4-difluoro-5-methyl-4-bora-3a,4a-diaza-s-indacene-3-dodecanoic acid (BODIPY D-3823, Molecular Probes). After 12 h continuous flow feeding in the incubator, the MPSs were imaged using a Nikon Eclipse TE300 fluorescence microscope equipped with a ORCA-Flash 4.0 CMOS Camera (Hamamatsu, Hamamatsu-city, Japan).

Confocal immunofluorescence microscopy was conducted on WAT chips that were fixed after 3 days and 9 days respectively of on-chip culture using 4% PFA for 30 min and a subsequent 1X PBS wash. Triton X-100 was used to permeabilize the cells followed by a 3% BSA blocking solution wash. After tissue fixation, 3T3-L1 cells were stained with DAPI (nuclei-blue), Phalloidin (Actin-GFP) and LipidTOX (lipid droplets-red). Confocal images were collected using a Carl Zeiss LSM 710 confocal microscope equipped with a plan-apochromat 10X/0.45 objective imaging DAPI (excitation 405 nm, emission: 410–494 nm), GFP (excitation 488 nm, emission: 493–550 nm), and LipidTOX red (excitation 595 nm, emission: 599–734 nm) channels.

For the visualization of the collagen in the ECM, picrosirius red staining (Polysciences Inc. Warrington, PA.) was used following the manufacturer protocol. Briefly, WAT chips were incubated for 1 h followed by two washes with an acetic acid solution. Bright field images were then collected using a Zeiss Axio Imager microscope (Carl Zeiss, Jena, Germany) equipped with a QImaging MicroPublisher 5.0 color camera (Q Imaging, Surrey, BC, Canada). On the images collagen appears red with a pale yellow background.

Results and Discussion

Concept of the microphysiological WAT-on-a-chip

To mimic the physiological environment of adipose tissue inside a microfluidic environment we have developed a microphysiological system that has three main elements: a media channel, circular cell chambers, and a microporous membrane in between. Analogous to the *in vivo* blood circulation, media travels through the media channel as a vasculature-like microcirculation between multiple WAT chambers and constantly transports fresh nutrients and other soluble factors (e.g. drug compounds, cytokines) to and metabolic waste and secreted factors away from the tissue (Fig. 1A). The media channel and WAT chambers are connected via small micropores (diameter 3 μm) that act as a perfusion barrier (Fig. 1B,C). The perfusion barrier mimics the *in vivo* endothelial barrier by allowing nutrients, drugs, and other media compounds to diffuse to the tissue while protecting the cells from shear stresses. The diffusion properties are regulated by the pore size and pore density. The circular geometry of the WAT chambers (diameter 600 μm, height 50 μm) creates a homogeneous supply with nutrients for the entire WAT tissue and enables the direct exchange of soluble factors with the media for each individual cell, which is important as *in vivo* each adipocyte is attached to at least one capillary.[46] Additionally, the microfluidic concept enables the temporal and lateral control of nanoliter fluid volumes and flows. The much smaller liquid volumes compared to standard cell culture further prevents non-physiological dilution of autocrine and paracrine factors. The basic principle of a vertically adjacent configuration of

separate media and tissue compartments enables a large degree of flexibility in terms of circulation architecture including in series- or in parallel-connections of multiple tissue chambers (Fig. 1D) interconnected by low dead-volume microchannels (width 40 μm, height 50 μm). Since the footprint of one tissue chamber is below 1 mm^2, it is possible to fabricate hundreds of cell chambers on a plate with standard multi-well plate dimension and thus enable high throughput screening. Another advantage of the microfluidics-based design is that the WAT-on-a-chip is amenable for characterization of a variety of structural and functional endpoints. For example, the optical accessibility of the tissue chamber enables the flexible use of high-resolution microscopy techniques for live cell imaging and the continuous media flow allows for temporal collection of the supernatant and subsequent analysis using for instance mass spectrometry or colorimetric assays. Additionally, the underlying concept permits the integration of the system in multi-organ circulations.[47]

Fabrication of the multilayer hybrid system

The media channel and the WAT chambers are patterned via UV-lithography and replica molded in two polydimethylsiloxane (PDMS) slabs, which constitute the lower and upper layers respectively of the three-layer hybrid MPS. The middle layer consists of an isoporous polyethylene terephthalate (PET) membrane. By choosing commercially available track-etched PET membranes, a variety of pore sizes and pore densities, viz. diffusion properties, can be employed without restriction by aspect-ratio limitations of UV-lithography and without changes in the actual fabrication process. Important for analysis methods requiring optical transparency, the choice of membranes with controlled angles of the pores is critical. To enable long-term tissue culture and the choice of a wide variety of fluidic parameters, a strong bonding of the three components is required. To achieve a coupling between the PET membrane and the PDMS devices, we employed a bis-amino-silane modification of the membrane recently introduced by Sip and Folch (Fig. 2A–C).[48] Note that many commercially available PET membranes are surface treated with PVP or other hydrophilic coatings, which will interfere with the coupling process. The advantage of this silane coupling approach is that the process solely requires commercially available reagents, is uniformly applied to surfaces and thus mostly feature-independent, and is compatible with PDMS oxygen plasma bonding. The silane treated membrane is sandwiched between two PDMS slabs, which have been activated via oxygen plasma (Fig. 2D). The components are then carefully aligned, brought into contact, and cured resulting in a bonded and sealed PDMS/PET hybrid system (Fig. 2E).

Characterization of transport processes

One of the major elements of the MPS is the separation of transport processes. In the human body, most tissues do not experience shear forces due to convective blood flow since they are protected by the endothelial barrier. Similarly, inside the MPS, the tissue is not subject to convective flow but is supplied by diffusive transport while the transport within the media channels is predominately convective (Fig. 3A). This is ensured by a narrow cross-section of the isoporous membrane with 3 μm diameter pores creating a fluidic resistance into the cell chamber significantly higher than through the media channel. The fluidic connection of cell and media channel as well as the different timescales of transport processes was shown using DI water colored with food dyes (Fig. 3B). This qualitative characterization

demonstrated that pumping a blue liquid into the media channels of a system entirely filled with red liquid leads to an immediate replacement of the liquid in the media channel and a subsequent color change in the cell chambers due to dye diffusion through the membrane.

Additionally, we employed quantitative theoretical models to demonstrate the desired transport separation effect. Using numerical analysis employing a “Transport of Diluted Species” model we assessed the concentration change in the cell chamber when pumping a liquid with a diffusive solute through the media channel. Due to the high computational costs of modeling the “small scale” membrane pores individually as well as the “large scale” channel structures, we employed a finite element model treating the membrane as a porous media. A time series of snapshots of the concentration distribution reveals a diffusive supply of media to the tissue on physiological timescales (Fig. 3C). Similarly, we simulated the flow fields in both the media channel and the cell chamber revealing the successful confinement of the convective flow as target and thereby confirming that the membrane effectively shields cells from the convective flow in the media channel and the resulting shear stress (Fig. 3D).

Independent of the numerical finite element model, we employed an analytical model which we developed based on a concept recently introduced by Chung *et al.*[42]: Application of the theoretical equations for our system results in a distribution of the flow rate in the cell chamber as shown in Fig. 3F and a maximum flow rate of less than 1/100 of the input flow rate in the media channel. Note that this value is independent of the width of the chamber and the fluidic viscosity of the media. Furthermore, taking into account that the tissue in the cell chamber will significantly increase the fluidic resistance, the actual flow rate in the tissue chamber will be even lower.

Taken together, both models provide qualitatively the same results although different approximations for the character of the membrane were used. Each model verified the separation of transport processes and thereby the shear stress protective effect of the membrane. The separation of transport processes providing a shear-force protection of the tissue is a key aspect of our system and serves as a recapitulation of the *in vivo* endothelial barrier. However, while providing mechanical support and controlled passive diffusion, the system does not fully mimic active transportation processes displayed by endothelial cells. Future systems with endothelial cells on the media-channel-side of the membrane can be envisioned to incorporate those processes as well. The choice of commercially available membranes, moreover, allows for the change of pore sizes, viz. diffusion properties, without changes in the actual fabrication process.

Injection and culture of functional adipose tissue

To create adipose tissue in the MPS, we obtained adipocytes by differentiating murine 3T3-L1 preadipocytes. Between 6–8 days after induction of adipogenesis, cells were harvested and loaded into the cell chambers of the MPS through small tree-like loading channels (width 80 μm, height 50 μm). Due to their fragility and buoyancy, adipocytes were more problematic than other cell types in terms of handling and compatibility with small-scale dimensions and shear stresses. Hence, an early injection time point was chosen, at which lipid droplets were clearly visible, but still small and sparsely distributed. Loaded chambers

were subsequently fed using a syringe pump induced continuous flow through the media channels. Within 24h of loading, the cells reattached and initiated the formation of a tissue.

An important prerequisite for the applicability of a WAT-on-a-chip MPS for drug screening applications is the capability to keep the tissue viable and functional over longer time periods, which we studied using a variety of approaches: as shown by Live/Dead cytotoxicity assays, (Fig. 4A,B) the MPS was able to keep the injected cells viable. Confocal immunofluorescence imaging further confirmed the 3D character of the adipose tissue in the MPS (Fig. 4C). To investigate the functionality of cells and the presence of cell-secreted ECM, an essential constituent of the 3D tissue, we performed picrosirius red staining visualizing collagen I and III at two different time points after cell loading (Fig. 4D). In-situ bright field microscopy characterization in 24h intervals clearly showed the expansion of cells and growth of lipid droplets indicating fully functional lipid metabolism by the adipose tissue (Fig. 5A). To visualize and confirm the lipid droplets, we employed a Bodipy 493/503 (D-3922, Molecular Probes) stain allowing us to detect the lipid droplets through standard epifluorescence and confocal microscopy (Fig. 5B). Our MPS, moreover, enabled the culture of adipose tissue for more than two weeks as demonstrated by the continuous growth of lipid droplets, indicating no loss of fatty acid uptake and triacylglycerol synthesis capabilities (Fig. 5C).

To directly assess relevant metabolic function, we visualized fatty acid uptake, a transporter mediated process[49] by incubating the MPS with medium containing a BSA-bound fluorescently-labeled long-chain fatty acid analog, i.e. C1-Bodipy-C12 500/510 (D-3823, Molecular Probes). Standard epifluorescence microscopy revealed that, two weeks after loading, large numbers of cells within the MPS showed significant uptake functionality (Fig. 5D). Thus, the MPS was capable of keeping adipose tissue viable and functional over longer time periods. Ultimately, our WAT MPS will enable additional physiological assays for lipids and glucose metabolism as well as insulin sensitivity and, given the small dimensions and potential for massive parallelization, our WAT MPS will allow for the rapid screening of adverse drug effects in complex metabolic systems. Down the road, the exploitation of microfabrication and microfluidic approaches provides the system with the potential for the integration with other microfluidic based organ systems. This will make the WAT MPS a powerful testbed opening a wide range of opportunities for fundamental biomedical studies as well as for translational applications in pharmaceutical industry.

Conclusion

We have developed a WAT-on-a-chip MPS that integrates adipose tissue in an environment which features crucial parts of the *in vivo* physiology such as continuous nutrient delivery and media exchange, spatially homogeneous nutrient supply, close proximity to the vasculature of each individual cell, separation of transport processes, as well as shear force protection for the tissue. Additionally, it has a low-cost character and is highly accessible for a variety of endpoint characterizations. The WAT MPS is capable of maintaining the viability and function of the tissue over multiple weeks. The highly controlled and computationally predictable character of the MPS make it a versatile tool for the study of

adipose tissue properties and responses to external stimulations, as well as adipose tissue associated diseases such as obesity and type 2 diabetes.

Acknowledgments

This research was supported by NIH grants UH2TR000487 (K.E.H.), UH2TR000487-02S1 (K.E.H. & A.S.), and UH3TR000487 (K.E.H.). P.L. was supported by a postdoctoral fellowship from the German Research Foundation, LO 2081/1-1. We acknowledge assistance from the Biomolecular Nanotechnology Center and the Marvell Nanofabrication Facility at UC Berkeley. Research was supported in part by the NIH S10 program under award number 1S10RR026866-01.

References

1. Mikos AG, Herring SW, Ochareon P, Elisseeff J, Lu HH, Kandel R, Schoen FJ, Toner M, Mooney D, Atala A, Van Dyke ME, Kaplan D, Vunjak-Novakovic G. Tissue Eng. 2006; 12:3307–3339. [PubMed: 17518671]
2. Berthiaume F, Maguire TJ, Yarmush ML. Annu Rev Chem Biomol Eng. 2011; 2:403–430. [PubMed: 22432625]
3. Scannell JW, Blanckley A, Boldon H, Warrington B. Nat Rev Drug discovery. 2012; 11:191–200. [PubMed: 22378269]
4. Marx, U., Sandig, V. Drug Testing In Vitro: Breakthroughs and Trends in Cell Culture Technology. 1. Wiley-VCH; Weinheim: 2007.
5. Baker M. Nature. 2011; 471:661–665. [PubMed: 21455183]
6. Huh D, Torisawa YS, Hamilton GA, Kim HJ, Ingber DE. Lab Chip. 2012; 12:2156–2164. [PubMed: 22555377]
7. Mathur A, Loskill P, Hong S, Lee JY, Marcus SG, Dumont L, Conklin BR, Willenbring H, Lee LP, Healy KE. Stem Cell Res Ther. 2013; 4(Suppl 1):S14. [PubMed: 24565415]
8. Bhatia SN, Ingber DE. Nat Biotechnol. 2014; 32:760–772. [PubMed: 25093883]
9. Mathur A, Loskill P, Shao K, Huebsch N, Hong S, Marcus SG, Marks N, Mandegar M, Conklin BR, Lee LP, Healy KE. Sci Rep. 2015; 5:8883–8883. [PubMed: 25748532]
10. Huh D, Matthews BD, Mammoto A, Montoya-Zavala M, Hsin HY, Ingber DE. Science. 2010; 328:1662–1668. [PubMed: 20576885]
11. Lee PJ, Hung PJ, Lee LP. Biotechnol Bioeng. 2007; 97:1340–1346. [PubMed: 17286266]
12. Jang KJ, Suh KY. Lab Chip. 2010; 10:36–42. [PubMed: 20024048]
13. Hsu YH, Moya ML, Hughes CCW, George SC, Lee AP. Lab Chip. 2013; 13:2990. [PubMed: 23723013]
14. Tanzi MC, Fare S. Expert Rev Med Devices. 2009; 6:533–551. [PubMed: 19751125]
15. Young, B., Woodford, P., O'Dowd, G. Wheater's Functional Histology. 6. Elsevier Health Sciences; 2013.
16. Trayhurn P, Beattie JH. Proc Nutr Soc. 2007; 60:329–339.
17. Scherer PE. Diabetes. 2006; 55:1537–1545. [PubMed: 16731815]
18. Kim SS, Moustaid-Moussa NN. J Nutr. 2000; 130:3110S–3115S. [PubMed: 11110881]
19. Shehzad AA, Iqbal WW, Shehzad OO, Lee YSY. Hormones (Athens). 2012; 11:8–20. [PubMed: 22450341]
20. Tilg H, Moschen AR. Nat Rev Immunol. 2006; 6:772–783. [PubMed: 16998510]
21. Rega-Kaun G, Kaun C, Wojta J. Thromb Haemostasis. 2013; 110:641–650. [PubMed: 23846791]
22. Blüher M, Mantzoros CS. Metabolism. 2015; 64:131–145. [PubMed: 25497344]
23. Buechler CC, Wanninger JJ, Neumeier MM. World J Gastroenterol. 2011; 17:2801–2811. [PubMed: 21734787]
24. Han SH, Quon MJ, Kim JA, Koh KK. JACC. 2007; 49:531–538. [PubMed: 17276175]
25. Jia T, Carrero JJ, Lindholm B, Stenvinkel P. Biochimie. 2012; 94:2150–2156. [PubMed: 22980197]
26. Nawrocki AR, Scherer PE. Drug Discov Today. 2005; 10:1219–1230. [PubMed: 16213414]

27. Ogden CL, Carroll MD, Kit BK, Flegal KM. NCHS Data Brief. 2012:1–8.
28. Lafuente-Lafuente C, Alvarez JC, Leenhardt A, Mouly S, Extramiana F, Caulin C, Funck-Brentano C, Bergmann JF. Br J Clin Pharmacol. 2009; 67:511–519. [PubMed: 19552745]
29. Poulin P, Schoenlein K, Theil FP. J Pharm Sci. 2001; 90:436–447. [PubMed: 11170034]
30. Choi JH, Gimble JM, Lee K, Marra KG, Rubin JP, Yoo JJ, Vunjak-Novakovic G, Kaplan DL. Tissue Eng Part B. 2010; 16:413–426.
31. Yao R, Du Y, Zhang R, Lin F, Luan J. Biomed Mater. 2013; 8:045005–045005. [PubMed: 23735623]
32. Mauney JR, Nguyen T, Gillen K, Kirker-Head C, Gimble JM, Kaplan DL. Biomaterials. 2007; 28:5280–5290. [PubMed: 17765303]
33. Wiggenhauser PS, Müller DF, Melchels FPW, Egaña JT, Storck K, Mayer H, Leuthner P, Skodacek D, Hopfner U, Machens HG, Staudenmaier R, Schantz JT. Cell Tissue Res. 2011; 347:747–757. [PubMed: 21850493]
34. Wang L, Johnson JA, Zhang Q, Beahm EK. Acta Biomater. 2013; 9:8921–8931. [PubMed: 23816649]
35. Tharp KM, Jha AK, Kraiczy J, Yesian A, Karateev G, Sinisi R, Dubikovskaya EA, Healy KE, Stahl A. Diabetes. 2015:db150728.
36. Frye CA, Patrick CW. In Vitro Cell Dev Biol Anim. 2006; 42:109–114. [PubMed: 16848629]
37. Guzzardi MA, Domenici C, Ahluwalia A. Tissue Eng Part A. 2011; 17:1635–1642. [PubMed: 21303256]
38. Godwin LA, Brooks JC, Hoepfner LD, Wanders D, Judd RL, Easley CJ. Analyst. 2015; 140:1019–1025. [PubMed: 25423362]
39. Viravaidya K, Shuler ML. Biotechnol Prog. 2008; 20:590–597.
40. Clark AM, Sousa KM, Chisolm CN, MacDougald OA, Kennedy RT. Anal Bioanal Chem. 2010; 397:2939–2947. [PubMed: 20549489]
41. Dugan CE, Kennedy RT. Meth Enzymol. 2014; 538:195–209. [PubMed: 24529440]
42. Chung HH, Chan CK, Khire TS, Marsh GA, Clark A, Waugh RE, McGrath JL. Lab Chip. 2014; 14:2456–19. [PubMed: 24850320]
43. Dagan Z, Weinbaum S, Pfeffer R. Chem Eng Sci. 1983; 38:583–596.
44. Hazel JR, Sidell BD. Anal Biochem. 1987; 166:335–341. [PubMed: 3434777]
45. Liao J, Sportsman R, Harris J, Stahl A. J Lipid Res. 2005; 46:597–602. [PubMed: 15547301]
46. Patrick CW. Seminars in Surgical Oncology. 2000; 19:302–311. [PubMed: 11135487]
47. Loskill P, Marcus SG, Mathur A, Reese WM, Healy KE. PLoS ONE. 2015; 10:e0139587. [PubMed: 26440672]
48. Sip CG, Folch A. Biomicrofluidics. 2014; 8:036504. [PubMed: 25379080]
49. Anderson CM, Stahl A. Molecular Aspects of Medicine. 2013; 34:516–528. [PubMed: 23506886]

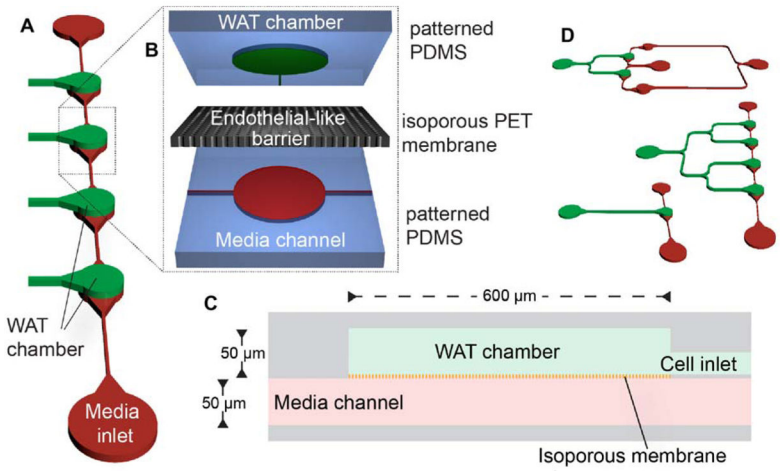

Fig. 1. Schematic concept of the WAT-on-a-chip

A) Scheme demonstrating the underlying idea of separated media channel and multiple individual WAT chambers. B) Schematic design and C) cross section of the multilayer PDMS-PET hybrid system. The MPS is based on a sandwich structure consisting of an isoporous PET membrane in between two PDMS layers, whereby the upper one features the WAT chamber (green) and the lower one the media channel (red). D) Examples of different circulation architecture versions connecting multiple cell chambers in series or in parallel.

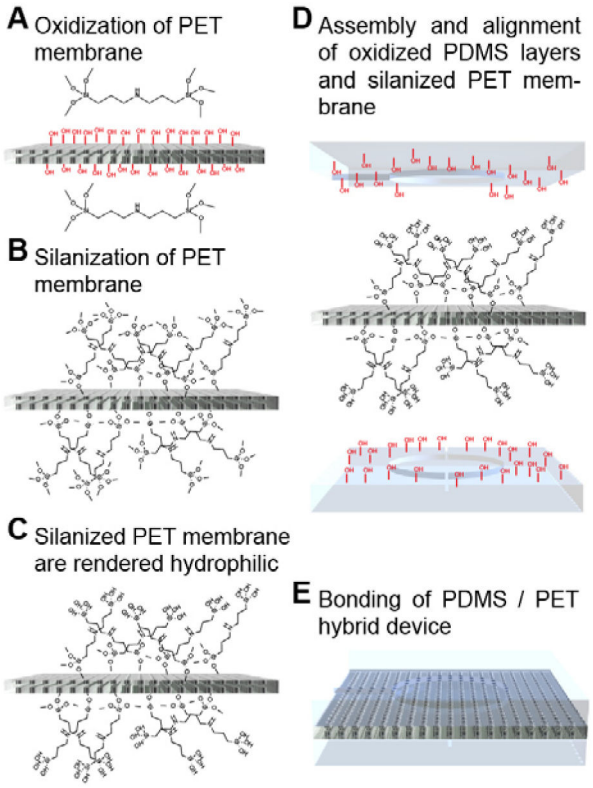

Fig. 2. Fabrication of the multilayer PDMS-PET hybrid MPS

A) An isoporous PET membrane is activated using O2 plasma and treated with a bis-amino silane solution at elevated temperature. The functionalized membrane is subsequently B) cured to further cross-link the silane layer and C) Hydrophilic coating via immersion in a 70% ethanol / water mixture. D) The silanized membrane is sandwiched between two activated PDMS layers, which are aligned under a stereoscope E) The PDMS / PET hybrid device is bonded, dried and baked.

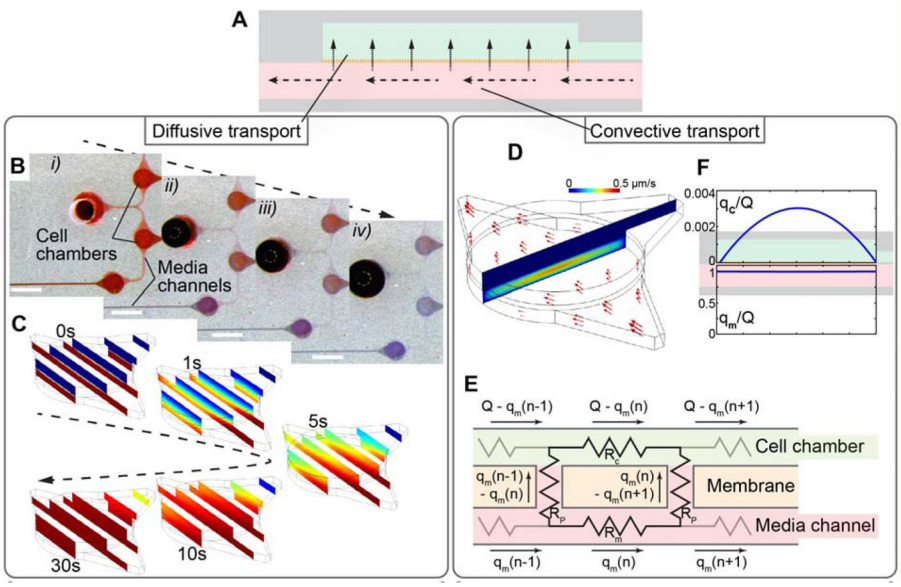

Fig. 3. Characterization of transport processes inside the MPS

A) Schematic view of the MPS highlighting the two different transport processes: convective flow within the media channel and purely diffusive transport to the tissue chamber. B) Time series of pictures at subsequent timepoints i)-iv) showing the replacement of red dyed water by injection of blue dyed water into the media channels. Note the subsequent change of colour in the cell chambers due to diffusion through the membrane. C) COMSOL simulation of the diffusion of small molecules from the media channel to the tissue chamber on physiological timescales. D) Schematic representation of the electrical circuit analogy using an idealized membrane on which the analytical model is based on. Adapted from Ref. 42. E) Input flow rate fraction in the tissue chamber along the flow axis calculated by the analytical model. F) Simulated velocity profile of flow in the MPS, inset shows the magnified view. Note the lack of convection within the diffusive barriers and predominant convective flow through the nutrient channels. Thus, mass transport to the tissue is exclusively diffusive.

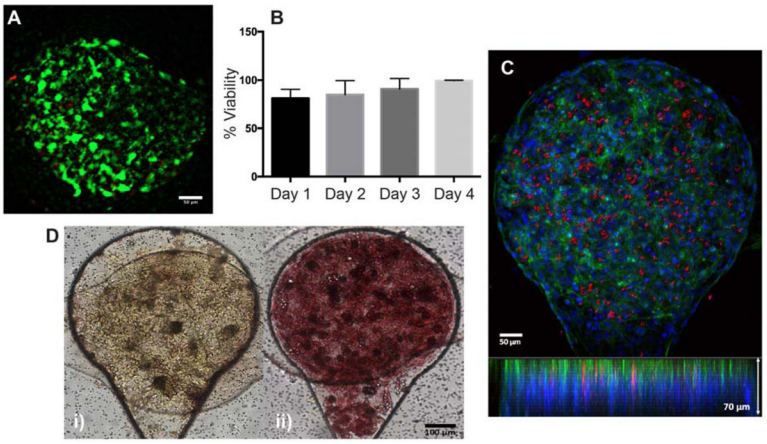

Fig. 4. Physiologically relevant adipose tissue in the MPS

A) Fluorescence microscopy image of a Live/Dead cytotoxicity assay after four days of on-chip culture. B) Quantification of the percentage of viable cells in the MPS at different time points of on-chip culture. C) Confocal image of 3T3-L1 adipocytes after 9 days in culture in the WAT MPS revealing a 3D tissue like structure. Cells were stained with phalloidin to show part of the cytoskeleton, DAPI to visualize the nuclei and LipidTOX red for the neutral lipid droplets. D) Bright field images of MPS's stained with picrosirius red after i) 3 days and ii) 9 days of on-chip culture showing a functional secretion of ECM (collagen), essential for a physiological tissue structure.

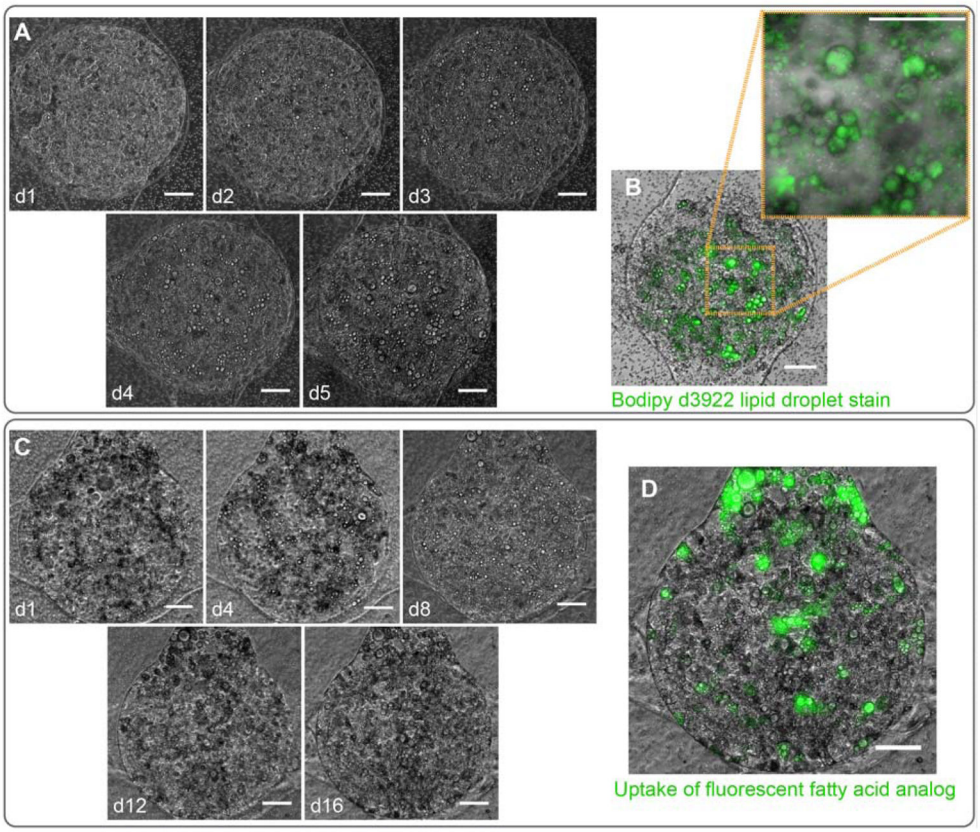

Fig. 5. The MPS enables maintenance of viability and functionality of adipose tissue

A) Series of optical microscopy images of a typical WAT chamber inside the MPS taken at subsequent days reveals the formation and growth of lipid droplets indicating functional fatty acid uptake. B) Fluorescent microscopy images inside an MPS stained six days after loading using a bodipy d3922 dye highlights the abundance of lipid droplet. C) Series of optical microscopy images shows formation and growth of lipid droplets for more than two weeks demonstrating the long-term culture capability of the MPS. D) Fluorescence microscopy image subsequent to exposure to the fluorescently labeled fatty acids analog C1-Bodipy-C12 confirming the fatty acid uptake ability and functionality of the tissue after two weeks on chip culture. (scalebars 100 μm)